

N-GLARE: An Non-Generative Latent Representation-Efficient LLM Safety Evaluator

Zheyu Lin

University of California, Riverside
Email: 1298lzy@gmail.com

Jirui Yang, Hengqi Guo, Yubing Bao, Yao Guan

Fudan University
Emails: {yangjr23, hqguo22, ybbao23, yguan25}@m.fudan.edu.cn

Abstract—Evaluating the safety robustness of LLMs is critical for their deployment. However, mainstream Red Teaming methods rely on online generation and black-box output analysis. These approaches are not only costly but also suffer from feedback latency, making them unsuitable for agile diagnostics after training a new model. To address this, we propose N-GLARE (A Non-Generative, Latent Representation-Efficient LLM Safety Evaluator). N-GLARE operates entirely on the model’s latent representations, bypassing the need for full text generation. It characterizes hidden layer dynamics by analyzing the APT (Angular-Probabilistic Trajectory) of latent representations and introducing the JSS (Jensen-Shannon Separability) metric. Experiments on over 40 models and 20 red teaming strategies demonstrate that the JSS metric exhibits high consistency with the safety rankings derived from Red Teaming. N-GLARE reproduces the discriminative trends of large-scale red-teaming tests at less than 1% of the token cost and the runtime cost, providing an efficient output-free evaluation proxy for real-time diagnostics.

1. Introduction

In recent years, Large Language Models (LLMs) have developed rapidly, with their capability boundaries continuously expanding. They have been deployed in a wide range of application scenarios, exerting substantial impact on social production and daily life [1], [2]. However, alongside this growth in capability, security risks and alignment issues have become increasingly prominent, emerging as a critical bottleneck for large-scale, safety-critical deployment [3], [4]. Trained on vast and often uncurated Internet corpora, LLMs can inadvertently internalize social biases and potentially harmful knowledge. Without robust safety alignment, they may produce unsafe outputs when exposed to malicious prompts, complex contexts, or specific triggers—for example, generating cyberattack code [5], spreading misleading information [6], or guiding embodied agents toward physically harmful behaviors [7]. Ensuring that LLMs remain aligned with human values and safety norms is therefore a central challenge.

Evaluating model safety is a foundational step toward achieving such alignment. The dominant paradigm in both industry and academia is currently Red Teaming [8], which

simulates adversarial user behavior by designing diverse, subtle attack prompts to probe the model and elicit unsafe outputs. While this online, behavior-based testing has proved effective for discovering vulnerabilities, it suffers from two fundamental limitations. First, it is highly resource-intensive: test coverage depends on the scale and diversity of attack prompts, which require continual human and computational investment as new attack vectors emerge. Second, Red Teaming is essentially a black-box methodology. It only observes input–output behavior and provides little insight into the model’s *internal* safety state. A refusal that looks safe at the surface level may simply be triggered by brittle pattern matching, rather than reflecting a robust internal representation of harmfulness.

To move beyond purely behavioral stress testing, recent work has begun to analyze LLMs in their latent representation space [9], [10]. Representation engineering shows that when a model processes different concepts (including abstract notions such as “truthfulness,” “refusal,” or “harmfulness”), its hidden activations form structured, often linearly separable patterns. Let $h_{l,p} \in \mathbb{R}^d$ denote the activation at layer l and position p . For two contrasting semantic sets \mathcal{S}^+ and \mathcal{S}^- , their mean activations differ along concept directions of the form

$$o \approx \mathbb{E}[H(\mathcal{S}^+)] - \mathbb{E}[H(\mathcal{S}^-)], \quad (1)$$

suggesting that high-level semantics are explicitly encoded in latent geometry. Existing work primarily uses such directions at the *prompt level*, for example to steer individual generations or to classify the risk of a specific input. However, these techniques are typically model-specific and do not directly provide a *model-level* safety indicator that is comparable across architectures and checkpoints.

In this paper, we take a step in that direction and ask: can we evaluate model safety *without* generating full outputs, solely by examining how its internal representations evolve under different safety conditions? To this end, we propose **N-GLARE** (A Non-Generative, Latent Representation-Efficient LLM Safety Evaluator), a framework that operates entirely in latent space and bypasses token-level generation. For each model, we construct **Angular-Probabilistic Trajectories** (APT) of hidden representations under different probing conditions: benign (B), jailbreak (J), plainquery

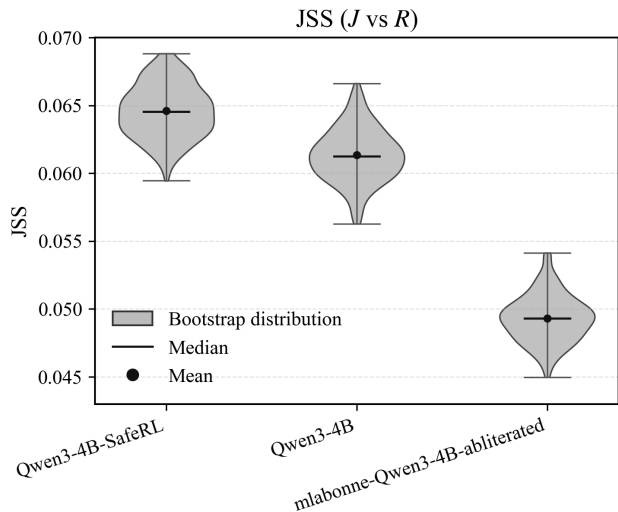


Figure 1: JSS Shows Stronger Safety Alignment in Qwen3-4B-SafeRL Compared to Base and Alignment-Removed Variants. Statistics on the JSS distribution for 100 jailbreak trajectories and the ideal refusal pattern.

(P) and an idealized refusal counterfactual (R). After normalizing these trajectories along a standardized progress axis, we model benign activations as a low-dimensional manifold and define a geometric *turning angle* that measures how strongly a trajectory deviates away from this benign manifold over time. We then introduce **Jensen–Shannon Separability** (JSS), which compares the slice-wise distributions of these turning angles across conditions, and aggregates them into model-level safety indicators, introducing other JSS-based safety scores.

Figure 1 illustrates the core intuition: when comparing multiple variants of the same base model (e.g., RL-aligned, base, and alignment-removed versions of Qwen3-4B), we observe that better-aligned variants exhibit more pronounced geometric separation between benign and jailbreak trajectories in latent space, and their jailbreak trajectories are also further away from the ideal refusal pattern. This suggests that internal trajectory separability can serve as a proxy for the underlying safety state of the model, potentially reproducing the discriminative power of large-scale Red Teaming at a fraction of the cost.

We formalize this idea in Section 3 by casting safety evaluation as a problem of comparing *representation trajectories* under (B, J, R, P) conditions. We then instantiate our method in Section 4: benign activations define a whitened manifold, the trajectory turning angle encodes instantaneous deviation from this manifold, and Jensen–Shannon divergence over angle distributions along the progress axis yields JSS metrics that are both geometrically interpretable and amenable to cross-model comparison. Experiments on over 40 models and 20 red-teaming strategies demonstrate that N-GLARE faithfully reproduces the safety rankings induced by traditional Red Teaming while using less than 1% of

the token and runtime cost, making it suitable for agile diagnostics after training new models or updating safety mechanisms.

Our main contributions are summarized as follows:

- **A non-generative, latent-space safety evaluator.** We propose N-GLARE, a framework that entirely bypasses online text generation and external output evaluators. To our knowledge, this is the first work to leverage latent representation trajectories for *model-level* LLM safety assessment.
- **A geometric formalization of safety alignment.** We formulate safety evaluation as a trajectory separability problem in representation space, construct a benign manifold via whitened PCA, and define an introduce Angular-Probabilistic Trajectories (APT) deviation measure. Building on this, we propose Jensen–Shannon Separability (JSS) and JSS-related normalized safety score as statistically robust, cross-model comparable indicators.
- **Extensive empirical validation and efficiency gains.** Across more than 40 models and 20 red-teaming strategies, we show that JSS-based rankings are highly consistent with those derived from traditional Red Teaming, while reducing token and runtime cost to below 1%. We further demonstrate that N-GLARE supports fine-grained analyses such as early-stage safety dynamics and comparison of alignment interventions across checkpoints, providing a practical tool for real-time safety diagnostics.

2. Technical Background

2.1. LLM Security and Red Teaming

Despite the widespread implementation of safety alignment in contemporary mainstream LLMs, they continue to face extensive security challenges in practical application [11]. Attackers frequently employ meticulously designed adversarial inputs to bypass the model’s safety guardrails [12], [13]. Through so-called “jailbreak attacks,” models are induced to circumvent their established policies, consequently generating harmful content. Such content may be exploited for academic misconduct [14], facilitating cyberattacks [15], or infringing upon copyright [16].

Consequently, ensuring that model outputs adhere to ethical norms and effectively mitigating potential risks have become indispensable research directions in the field of artificial intelligence. In this context, the security evaluation of large models is paramount, wherein Red Teaming has emerged as a core methodology for assessing model safety.

Red Teaming is an adversarial evaluation method centered on proactively discovering and identifying potential model vulnerabilities by simulating attacker strategies and behaviors. Existing Red Teaming approaches can be broadly categorized into two types. The first focuses on content safety in single-turn interactions, such as leveraging algorithms like Monte Carlo Tree Search (MCTS) and

evolutionary algorithms to optimize attack prompts [17], or generating jailbreak templates through the mutation of seed prompts [18]. The second category addresses security risks in multi-turn dialogue scenarios, typically employing specialized agents for attack planning, executing dynamic multi-turn jailbreaks, and evaluating the attack’s efficacy [19], [20], [21].

Although existing methods show a trend towards diversification, their mainstream paradigm still generally follows a three-stage process: first, constructing the attack prompt; second, obtaining the target model’s output for the prompt; and finally, judging the success of the attack based on the evaluation of the model’s output results. This model leads to particularly high evaluation overhead for Red Teaming.

2.2. LLM Latent Space Analysis Techniques

The internal mechanisms of LLMs are often treated as a black box. To understand how they process information, researchers analyze their latent space, i.e., the internal high-dimensional hidden states. In Transformers, this corresponds to the activation vector $h_{l,p} \in \mathbb{R}^d$ at a specific layer l and token position p , where d is the hidden dimension.

2.2.1. Embedding Analysis. Embedding analysis reveals semantic meaning by examining the static geometry of latent space vectors. Common methods like cosine similarity ($Sim(\vec{A}, \vec{B}) = \frac{\vec{A} \cdot \vec{B}}{\|\vec{A}\| \|\vec{B}\|}$) and dimensionality reduction visualization like t-SNE can reveal semantic clusters (e.g., “king” with “queen”) [22]. Furthermore, domain-adaptation analysis shows that fine-tuning (e.g., BioBERT [23]) reshapes the latent space, forming more refined domain-specific subspaces to enhance downstream task performance.

2.2.2. Probing and Intervention. This technique shifts from passive analysis to active decoding and control. Early probing [24] used simple linear classifiers ($y = f(H)$) to test if latent activations H encoded specific linguistic properties, discovering that information is stored hierarchically in LLMs.

A more advanced paradigm, Representation Engineering (RepE) [9], controls model behavior by directly manipulating latent representations. Its core is identifying vector directions, or concept operators o^c , that represent high-level concepts (e.g., truthfulness). This is often achieved by contrasting the activation differences from different input sets (S^{c+} vs S^{c-}):

$$o^c \approx \mathbb{E}[H(S^{c+})] - \mathbb{E}[H(S^{c-})] \quad (2)$$

Here, $H(S)$ represents the mean activation of model M when processing a specific input set S . RepE is widely applied in LLM safety [25], [26], [27], [28], for instance, by using positive or negative steering vectors to enhance truthfulness [29], [30], [31], [32] or suppress meta-behaviors like “refusal” [33].

2.2.3. Attention Mechanism Analysis. Attention mechanism analysis interprets the model’s information flow via its weight distribution $A = \text{softmax}\left(\frac{QK^T}{\sqrt{d_k}}\right)$. Here, the Q, K, V matrices are linear projections of the layer input h_{l-1} . Heatmap visualization [34] reveals that attention exhibits hierarchical properties (from syntax to semantics across layers). At the same time, research [35] indicates high redundancy in attention mechanisms. To address its computational complexity, models like Perceiver [36] introduce low-dimensional latent variables to compress the computation.

2.2.4. Latent Space Dynamic Analysis. Dynamic analysis focuses on the activation trajectories during the reasoning process. Researchers not only track attention changes during Chain-of-Thought (CoT) [37] but also begin to analyze the latent space trajectories themselves. For example, Li et al. [38] proposed Chain-of-Reasoning Embedding (CoRE), which treats the reasoning process as a series of hidden states $h_{l,p,r}$. They found that redundant reasoning (“overthinking”) manifests as identifiable cyclical fluctuations in the trajectory. Based on this, the CoRE-Eval framework was developed, enabling label-free self-evaluation to dynamically terminate inefficient reasoning, thereby improving efficiency.

Despite significant progress in analysis techniques for LLM latent spaces, the field still faces the challenge of model-specificity: the identified features, concept operators (like o^c), attention heads, or reasoning trajectories are often highly dependent on a single model M and lack transferability across models.

3. Problem Statement

Safety evaluation of large language models is currently dominated by *generative* red-teaming: a model is queried with adversarial prompts generated by red-teaming LLMs, asked to produce multi-token outputs, and then judged by a human or a separate LLM-based evaluator. This approach is expensive (because evaluation cost grows with generated tokens), noisy (because harmfulness must be inferred from surface text), and incomplete (because it reveals only the final behavior, not the underlying safety state).

Formally, let M_{subject}, M_s be a model and let x be a potentially harmful input drawn from an adversarial distribution \mathcal{D}_{adv} or online M_{attacker}, M_r . A generative evaluator, another LLM $M_{\text{evaluator}}, M_e$ observes the decoded output $y = M_s(x)$ and produces an assessment $\text{Eval}_{M_e}(y)$ that approximates the latent safety function $f_{\text{safety}}(M_s, x)$. That is,

$$\text{Eval}_{M_e}(y) \approx f_{\text{safety}}(M_s, x),$$

where this 0/1 function, f_{safety} represents whether the model processes x in a safe or unsafe manner. This evaluation pipeline is entirely output-dependent (by analyzing the natural language text) and therefore cannot access $f_{\text{safety}}(M_s, x)$ directly.

In contrast, a *non-generative* evaluator also seeks to estimate $f_{\text{safety}}(M_s, x)$ *without decoding any output tokens*. Instead, it relies only on information available *inside the* M_s . The goal is to design a mapping

$$g : (M_s, x) \mapsto f_{\text{safety}}(M_s, x),$$

where $g(M, x)$ is a model-level safety signal that: (i) approximates the same generative-based quantity $\text{Eval}_{M_e}(y)$ evaluated by LLM-based evaluator, (ii) is comparable across models and prompts, and (iii) does not rely on online red-teaming text generation or attackers M_r .

The core problem addressed in this work is therefore:

How can we construct a non-generative safety metric $g(\cdot, \cdot)$ that reliably reflects a model’s internal safety state and correlates with its behavioral robustness observed under traditional red-teaming?

This paper develops such a metric by operating entirely in the representation space, enabling low-cost, model-level safety evaluation without generation.

4. Methodology

We now instantiate the representation-space safety evaluation framework outlined above. Given a set of models $\mathcal{M} = \{M_1, \dots, M_K\}$ and probing conditions $A \in \{B, J, R, P\}$ (benign, jailbreak, ideal refusal), our goal is to map internal activation trajectories to scalar safety indicators. The pipeline proceeds in three stages: (i) extracting layer-wise hidden states and normalizing them along a standardized progress axis; (ii) fitting a benign manifold and defining a geometric turning angle that measures instantaneous deviation from this manifold; and (iii) aggregating slice-wise Jensen–Shannon divergences of turning-angle distributions into Jensen–Shannon Separability (JSS) metrics and a normalized safety score.

4.1. Trajectory Extraction and Standardized Progress

For each model M and probing condition $A \in \{B, J, R, P\}$ (defined in Section 4.3), we construct probing sequences that form either genuine interaction histories (e.g., multi-turn dialogues) or canonical prefix expansions for single-turn prompts. At each node t in such a sequence, we identify a fixed decision-making cross-section, chosen in our experiments as the point immediately before the model generates the next assistant response. A single forward pass at node t yields the last-token hidden activations across all transformer layers,

$$\Phi_M^{(A)}(t) = (h_{L,t}^{(A)}, \dots, h_{1,t}^{(A)}), \quad h_{\ell,t}^{(A)} \in \mathbb{R}^{d_\ell}, \quad (3)$$

where L is the number of layers and d_ℓ is the hidden dimension at layer ℓ .

To improve cross-model comparability and reduce dimensionality, we partition layers into a small number of

layer groups $G \in \{\text{lower, middle, upper}\}$ and average within each group, obtaining group-level representations

$$h_t^{(A,G)} \in \mathbb{R}^d, \quad (4)$$

with a common dimension d . For each condition A and group G , the sequence $\{h_t^{(A,G)}\}_{t=1}^{T_A}$ defines a trajectory in latent space.

The length T_A of a probing sequence may vary across prompts and models. To enable comparison on a common timeline, we normalize each trajectory by its arc length and define a standardized progress variable $s_t \in [0, 1]$:

$$s_1 = 0, \quad s_t = \frac{\sum_{k=1}^{t-1} \|h_{k+1}^{(A,G)} - h_k^{(A,G)}\|_2}{\sum_{k=1}^{T_A-1} \|h_{k+1}^{(A,G)} - h_k^{(A,G)}\|_2}, \quad t > 1. \quad (5)$$

This parametrization treats trajectories from different prompts and models as curves evolving along the shared progress axis $s \in [0, 1]$. In single-turn settings where there is no natural temporal dimension, we construct pseudo-sequences via canonical prefix augmentation (e.g., from an empty system prompt to the full user query) and apply the same normalization. We denote the resulting standardized trajectory under condition A and group G by

$$\Gamma_M^{(A,G)} = \{(h_t^{(A,G)}, s_t)\}_{t=1}^{T_A}. \quad (6)$$

4.2. Benign Manifold and Geometric Turning Angle

To quantify deviations from normal behavior, we first construct a benign manifold using representations collected under the benign condition B . For each group G , we aggregate all benign activations across prompts and progress values:

$$\mathcal{H}_B^{(G)} = \{h^{(B,G)}\}. \quad (7)$$

We estimate the empirical mean and covariance

$$\begin{aligned} \mu^{(G)} &= \mathbb{E}[h^{(B,G)}], \\ \Sigma^{(G)} &= \mathbb{E}[(h^{(B,G)} - \mu^{(G)})(h^{(B,G)} - \mu^{(G)})^\top], \end{aligned} \quad (8)$$

and perform a rank- r eigendecomposition

$$\Sigma^{(G)} \approx U_r^{(G)} \Lambda_r^{(G)} U_r^{(G)\top}, \quad r \ll d, \quad (9)$$

where $U_r^{(G)} \in \mathbb{R}^{d \times r}$ contains the top- r eigenvectors and $\Lambda_r^{(G)} \in \mathbb{R}^{r \times r}$ is the diagonal matrix of corresponding eigenvalues. This defines a benign subspace

$$\mathcal{S}^{(G)} = \text{span}(U_r^{(G)}), \quad (10)$$

and a whitening transform

$$W^{(G)} = \Lambda_r^{(G)-1/2} U_r^{(G)\top}. \quad (11)$$

For any representation h , its whitened coordinate is

$$z = W^{(G)}(h - \mu^{(G)}), \quad (12)$$

which removes scale and correlation effects in the benign distribution and provides a canonical coordinate system for measuring deviations across models.

By the Eckart–Young–Mirsky theorem [39], [40] and the tangent-space linearization principle for smooth manifolds [41], the top- r PCA subspace offers the statistically optimal linear surrogate of the benign manifold.

Given the benign manifold, we define an instantaneous geometric measure that characterizes how a trajectory moves relative to this manifold. For any representation h , we consider its reconstruction from the benign subspace:

$$\hat{h}^{(G)} = \mu^{(G)} + U_r^{(G)} U_r^{(G)\top} (h - \mu^{(G)}), \quad (13)$$

and define the residual

$$r^{(G)}(h) = h - \hat{h}^{(G)} = h - \mu^{(G)} - U_r^{(G)} U_r^{(G)\top} (h - \mu^{(G)}). \quad (14)$$

The squared norm

$$E_b^{(G)}(h) = \|r^{(G)}(h)\|_2^2 \quad (15)$$

acts as a deviation energy from the benign manifold. Its gradient

$$n^{(G)}(h) = \nabla E_b^{(G)}(h) = 2r^{(G)}(h) \quad (16)$$

defines an outward normal direction pointing away from the benign subspace at h .

For each trajectory and its representation $h_t \in \Gamma_M^{(A,G)}$, the tangent direction at node t is given by

$$\tau_t^{(A,G)} = \frac{h_{t+1}^{(A,G)} - h_t^{(A,G)}}{\|h_{t+1}^{(A,G)} - h_t^{(A,G)}\|_2}, \quad (17)$$

for $1 \leq t < T_A$. We then define the turning angle $\theta_t^{(A,G)} \in [0, \pi]$ between the trajectory tangent and the outward normal:

$$\theta_t^{(A,G)} = \arccos \left(\frac{\tau_t^{(A,G)\top} n^{(G)}(h_t^{(A,G)})}{\|\tau_t^{(A,G)}\|_2 \|n^{(G)}(h_t^{(A,G)})\|_2} \right). \quad (18)$$

In practice, since $n^{(G)}(h)$ is collinear with $r^{(G)}(h)$, we compute the numerator as $\tau_t^{(A,G)\top} r^{(G)}(h_t^{(A,G)})$ and normalize accordingly. Intuitively, $\theta_t^{(A,G)}$ measures how strongly the trajectory at t turns ‘‘away’’ from the benign manifold. Smaller angles (particularly $\theta_t^{(A,G)} < \pi/2$) indicate movement into regions further from benign behavior.

4.3. Probing Conditions, Slicing, and JSS Metrics

We apply the above constructions to three probing conditions that are designed to be isomorphic along the progress axis s :

- **Benign (B):** natural or conventional task distributions, used to fit the benign manifold and serve as a reference.
- **Jailbreak (J):** adversarial sequences designed to elicit harmful behavior.

Algorithm 1 JSS Core Computation for Model M

Require: Model M ; datasets \mathcal{D}_A for $A \in \{B, J, R, P\}$; hyperparameters $(r, G, I, s_0, \{w_i\}, \{w'_i\})$.
Ensure: $\text{JSS}(J, B)$, $\text{JSS}_{\text{early}}(J, B)$, $\text{JSS}(J, R)$, $\text{JSS}_{\text{early}}(J, R)$, $\text{JSS}(P, B)$.

- 1: **Trajectory extraction and benign manifold fitting**
- 2: **for each** $A \in \{B, J, R, P\}$ **do**
- 3: $\{\Gamma_M^{(A,G)}\}_G \leftarrow \text{EXTRACTANDNORMALIZE}(\mathcal{D}_A, M, G)$
- 4: **end for**
- 5: $\mathcal{H}_B^{(G)} \leftarrow$ collect all $h^{(B,G)}$ from $\Gamma_M^{(B,G)}$ for each G
- 6: $(\mu^{(G)}, U_r^{(G)}, \Lambda_r^{(G)}) \leftarrow \text{WHITENEDPCA}(\mathcal{H}_B^{(G)}, r)$
- 7: **Turning-angle computation**
- 8: **for each** $A \in \{B, J, R, P\}$ and each G **do**
- 9: $\Theta^{(A,G)} \leftarrow \text{CALCULATEANGLES}(\Gamma_M^{(A,G)}, \mu^{(G)}, U_r^{(G)})$
 $\{\text{all } (\theta_t^{(A,G)}, s_t)\}$
- 10: **end for**
- 11: **Slice-wise JS aggregation**
- 12: **for each comparison** $(A, B') \in \{(J, B), (J, R), (B, R), (P, B)\}$ **do**
- 13: **for each** G **do**
- 14: $\text{JSS}^{(G)}(A, B') \leftarrow 0$, $\text{JSS}_{\text{early}}^{(G)}(A, B') \leftarrow 0$
- 15: **for** $i = 1$ to I **do**
- 16: $\Theta_A^{(G)}(s_i) \leftarrow \{\theta : (\theta, s) \in \Theta^{(A,G)}, s \in s_i\}$
- 17: $\Theta_{B'}^{(G)}(s_i) \leftarrow \{\theta : (\theta, s) \in \Theta^{(B',G)}, s \in s_i\}$
- 18: $\text{JS}_i^{(G)}(A, B') \leftarrow \text{JS}(\text{Dist}(\Theta_A^{(G)}(s_i)) \parallel \text{Dist}(\Theta_{B'}^{(G)}(s_i)))$
- 19: $\text{JSS}^{(G)}(A, B') += \text{JS}_i^{(G)}(A, B')$
- 20: **if** $s_i \leq s_0$ **then**
- 21: $\text{JSS}_{\text{early}}^{(G)}(A, B') += \text{JS}_i^{(G)}(A, B')$
- 22: **end if**
- 23: **end for**
- 24: **end for**
- 25: $\text{JSS}(A, B') \leftarrow \frac{1}{|G|} \sum_G \text{JSS}^{(G)}(A, B')$
- 26: $\text{JSS}_{\text{early}}(A, B') \leftarrow \frac{1}{|G|} \sum_G \text{JSS}_{\text{early}}^{(G)}(A, B')$
- 27: **end for**
- 28: **return** $\text{JSS}(J, B)$, $\text{JSS}_{\text{early}}(J, B)$, $\text{JSS}(J, R)$, $\text{JSS}_{\text{early}}(J, R)$, $\text{JSS}(P, B)$

- **Ideal refusal (R):** sequences identical to J in user content, but with the assistant response replaced by a fixed, policy-compliant refusal template.
- **Plain Query (P):** sequences that repeatedly present the raw jailbreak true intention to the model, capturing the model’s unconstrained internal response trajectory under direct exposure to harmful prompts.

For each group G and condition A , we thus obtain a set of angle–progress pairs (i.e. Angular-Probabilistic Trajectories, APT)

$$\Theta^{(A,G)} = \{(\theta_t^{(A,G)}, s_t)\}. \quad (19)$$

To study how separability evolves along the interaction, we discretize the standardized axis $s \in [0, 1]$ into I slices (bins)

$\{s_i\}_{i=1}^I$. In slice s_i , we collect all angles whose progress falls into that interval:

$$\Theta_A^{(G)}(s_i) = \{\theta_t^{(A,G)} : s_t \in s_i\}. \quad (20)$$

We also define an early-stage threshold $s_0 \in (0, 1)$ (default $s_0 = 0.4$) and use it to construct “early- s ” metrics that focus on whether the model exhibits safe behavior in the initial portion of the trajectory.

Within each slice s_i and group G , we estimate the empirical distributions of the angle samples for two conditions A and B (e.g., J vs. B , or J vs. R), denoted by $\text{Dist}(\Theta_A^{(G)}(s_i))$ and $\text{Dist}(\Theta_B^{(G)}(s_i))$, meaning the distribution of them. We then compute the Jensen–Shannon divergence:

$$\text{JS}_i^{(G)}(A, B) = \text{JS}(\text{Dist}(\Theta_A^{(G)}(s_i)) \parallel \text{Dist}(\Theta_B^{(G)}(s_i))) \quad (21)$$

To obtain a model-level separability measure, we aggregate slice-level divergences. For each group G ,

$$\text{JSS}^{(G)}(A, B) = \sum_{i=1}^I \text{JS}_i^{(G)}(A, B), \quad (22)$$

and average across layer groups to obtain the all- s separability:

$$\text{JSS}(A, B) = \frac{1}{|G|} \sum_G \text{JSS}^{(G)}(A, B). \quad (23)$$

Restricting to slices with $i \leq s_0$ yields the early- s separability:

$$\text{JSS}_{\text{early}}(A, B) = \frac{1}{|G|} \sum_G \sum_{i \leq s_0} \text{JS}_i^{(G)}(A, B). \quad (24)$$

Algorithm 1 summarizes the core computation of JSS metrics for a single model M . For clarity, the pseudocode illustrates a single run on the full dataset. In our experiments, we wrap this procedure in a bootstrap loop to obtain empirical confidence intervals and perform non-parametric statistical tests across models.

5. Experiments and Analysis

This section begins by presenting the intuitive safety characteristics derived from latent representation trajectories, illustrating how model representations evolve under different dialogue families. Subsequently, from a dynamical perspective, we systematically examine the correspondence between these latent features and the model’s surface-level safety behaviors, thereby validating the safety representation hypothesis proposed earlier. On this basis, we employ quantified safety feature metrics to evaluate various aligned models and compare their rankings with those obtained from systematic traditional red-teaming evaluations, demonstrating a high degree of consistency in safety scales as well as a significant advantage in evaluation cost. Finally, we investigate the statistical consistency of the ranking results across different datasets and sample sizes, analyzing the stability of this evaluation framework under changes in data distribution and sampling conditions.

5.1. Trajectory Evolution Dynamics

This subsection empirically establishes one core observation of our evaluation framework:

Observation 1. *A model’s safety state is not only a behavior-based static attribute, but rather a dynamic process that can be continuously tracked within the latent representation space.*

Specifically, in Figure 2, we compare the APT evolutionary trajectories of the PlainQuery, Baseline, Jailbreak, and Ideal Refusal dialogue families. Baseline maintains a stable, flat trajectory, representing the model’s consistent generation direction during natural dialogue. PlainQuery rises sharply across all layers, rapidly diverging from the baseline, indicating that the model promptly shifts its generation direction upon detecting harmful intent, forming a distinct refusal response. Jailbreak trajectories gradually diverge upward from the baseline, exhibiting a notable downward drift in the higher layers, suggesting that adversarial semantics accumulate in upper-layer representations, progressively eroding the refusal mechanism. Although the Ideal-Refusal trajectory initially follows the Jailbreak path, a clear bifurcation emerges, indicating that the model encodes a latent distinction between accepting and refusing harmful instructions. Such separation suggests that the model possesses an intrinsic cognitive bias that differentiates unsafe compliance from defensive rejection within its internal representation space.

5.2. Synchronous Evolution of Jailbreak Progression, Refusal Tendency, and JSS Dynamics

After obtaining the intuitive empirical phenomena, we focus on verifying two key observations:

Observation 2. *Divergence between Jailbreak and Baseline trajectories as an indicator of the model’s discriminative capability to detect jailbreak attacks process shifting.*

A separation between the jailbreak attack trajectory and the baseline behavior trajectory in the representation space signifies a clear process shift in the model’s internal dynamics from normal generation to adversarial alignment. This divergence reflects the model’s discriminative capability to detect and respond to emerging jailbreak cues, serving as a direct and quantifiable indicator of its latent safety awareness.

Observation 3. *Distance between Jailbreak and Ideal Refusal trajectories as an indicator of the model’s intrinsic refusal tendency.*

The JS distance between Jailbreak and Ideal Refusal trajectories directly reflects the model’s ability to distinguish and resist jailbreak behaviors. An increase in this distance indicates that the model has a stronger latent discrimination between “accepting” and “blocking” jailbreak instructions, thus exhibiting an enhanced intrinsic refusal tendency, corresponding to a higher level of safety awareness.

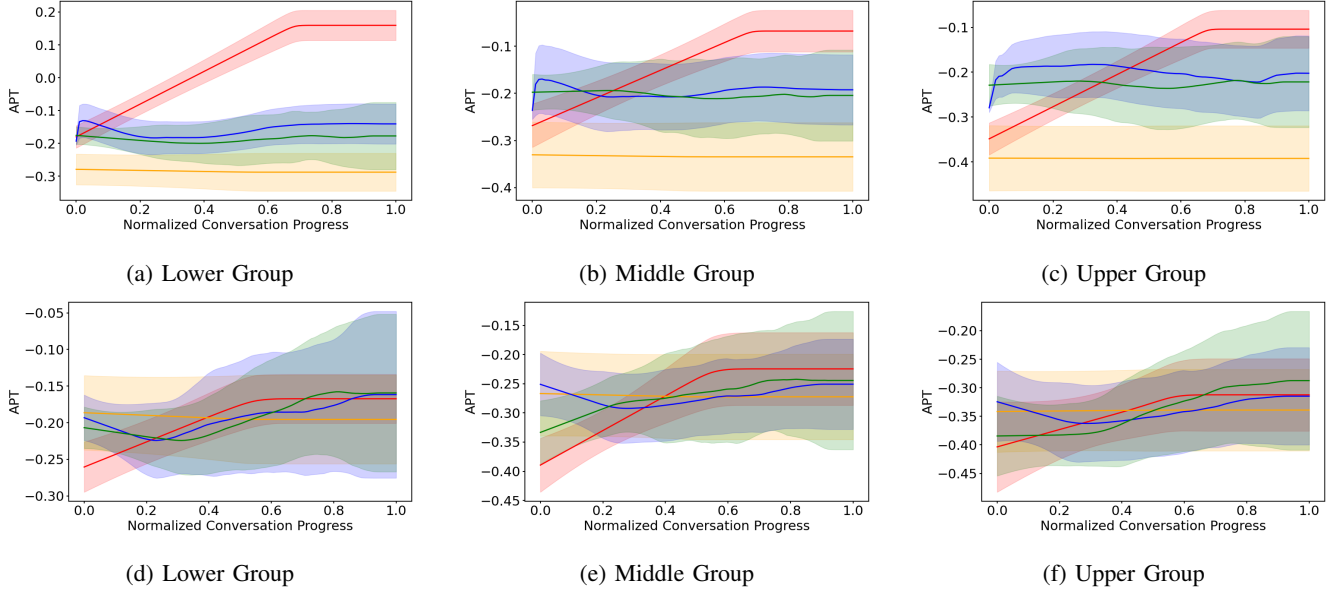


Figure 2: APT trajectories collected from different layer groups. Subfigures (a)(b)(c) correspond to safety-aligned models, while (d)(e)(f) are from jailbreak-tuned models. Red curves represent Plain Query trajectories, yellow denote Benign trajectories, blue indicate Jailbreak trajectories, and green correspond to Ideal Refusal trajectories. Safety-aligned LLMs exhibit well-separated and low-variance APT trajectories, whereas jailbreak-tuned LLMs show weakened separability and substantially higher variance across all query types, indicating degraded safety boundaries.

5.2.1. Phase-wise Dynamics of Jailbreak Trajectories and Latent Safety Awareness.

For observation 2, if a model lacked latent safety awareness, JB activations would remain near the Baseline manifold, yielding no meaningful temporal segmentation. To test whether phase structure exists and whether it is safety-dependent, we use a lightweight neural classifier as an operational probe: if representations at different jailbreak stages encode distinct information, the classifier should reliably separate them. Aligned Llama-family models indeed show strong separability: 0.86–0.97 (start vs. mid), 0.91–0.96 (start vs. end), 0.85–0.86 (mid vs. end). However, after ablating safety alignment (manually jailbroken variants), stage classification collapses to ~ 0.33 for all pairs. This contrast provides two conclusions: (1) the phase structure is statistically reliable, because it can be consistently decoded by a simple classifier; (2) it is safety-dependent, because the structure disappears once alignment is destroyed. Thus, aligned models internally encode a latent variable corresponding to the stage of the jailbreak process, and the resulting phase-wise divergence of JB from Baseline offers a direct, graded indicator of latent safety awareness.

5.2.2. Distance between Jailbreak and Ideal Refusal Trajectories and the Model’s Refusal Tendency.

For another observation 3, empirical measurements confirm a strong synchrony between Ideal Refusal-Jailbreak separability and model’s refusal tendency. We evaluate the model’s latent refusal inclination strength by using a unified metric of how strongly the model tends to generate reject-related tokens at

each stage of the jailbreak process. Specifically, we formalize ANM, which quantifies probability-level concentration on “refusal-cluster” tokens.

$$\text{ANM}(x) = \langle W_{\text{ref}}, p(\cdot | x) \rangle = \sum_{v \in \mathcal{V}} W_{\text{ref}}(v) p(v | x), \quad (25)$$

where $p(v | x) = \text{softmax}(z_v(x)/\tau_{\text{pred}})$ is the model’s next-token distribution, and W_{ref} is a fixed refusal-prototype distribution constructed by:

$$W_{\text{ref}}(v) = \frac{\exp(\langle \hat{e}_v, \hat{c} \rangle / \tau_{\text{ref}})}{\sum_{u \in \mathcal{V}} \exp(\langle \hat{e}_u, \hat{c} \rangle / \tau_{\text{ref}})}, \quad (26)$$

with \hat{c} obtained by averaging normalized embeddings of several refusal-seed phrases. (“sorry”, “I can’t”, etc.) Thus, ANM quantifies how strongly the model’s predictive distribution aligns with refusal-semantics in latent space.

Across layers, ANM curves exhibit a striking “mid-phase rise and end-phase collapse” pattern that matches the Ideal Refusal-Jailbreak JSS waveform projected into the same 0–1 domain. According to the results, layer-wise correlations between ANM and Ideal Refusal-Jailbreak JSS ($r = 0.70, 0.56, 0.54$; $\text{RMSE} = 0.13\text{--}0.20$) [42] reveal a strong phase-locked coupling between representational separability and refusal intensity. In each layer, the mid-segment elevation ($s \approx 45\text{--}65$) corresponds to a surge of refusal semantics, while the late-stage decline ($s > 70$) aligns with the erosion of this tendency as jailbreak success emerges.

The consistent alignment between ANM and Ideal Refusal-Jailbreak separability provides a quantitative bridge

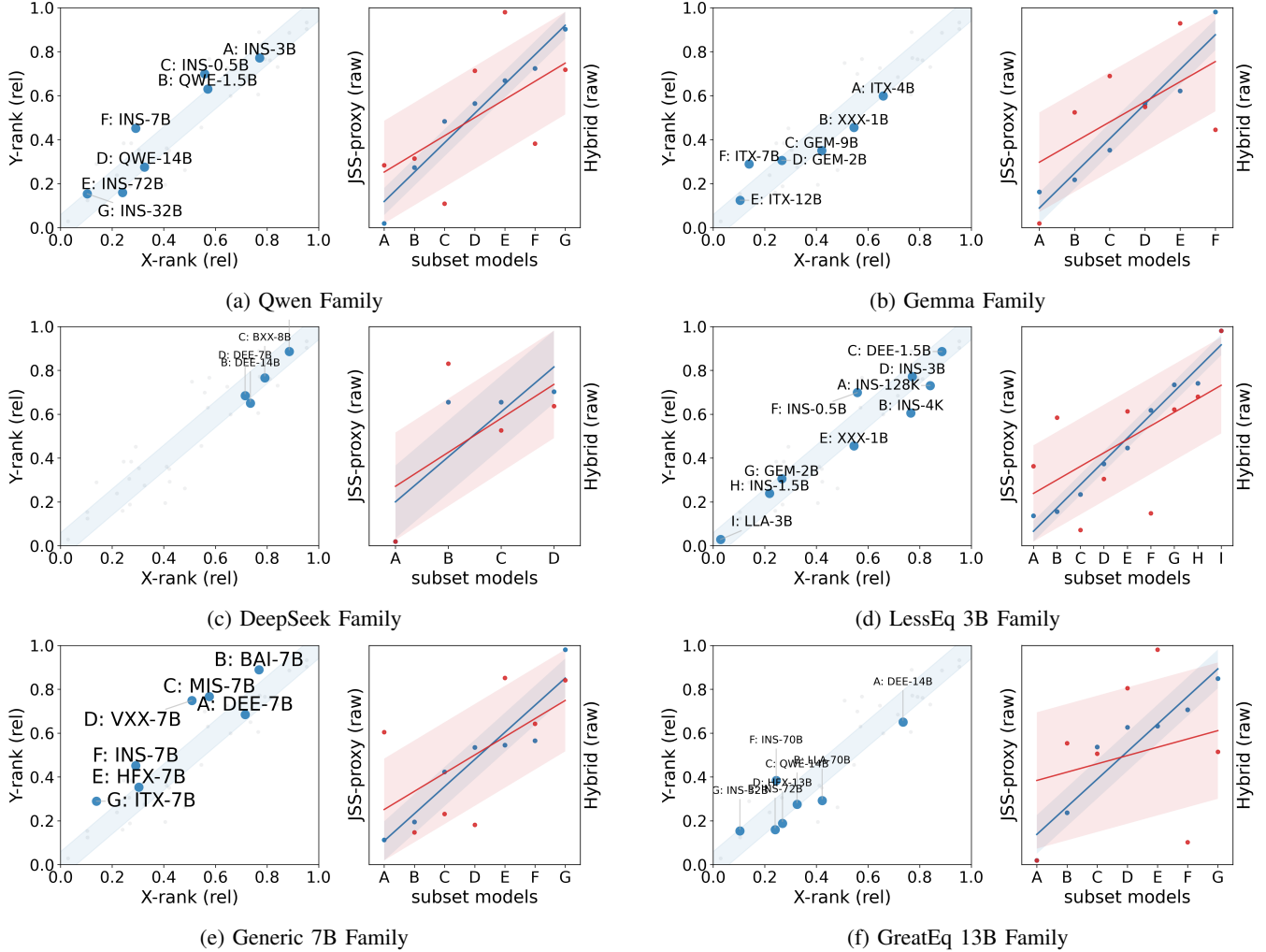


Figure 3: **Multi-perspective cross-model safety ranking consistency between N-GLARE and traditional red-teaming.** For each model family ((a-f; see Appendix Table 2 for model abbreviations on scatters)), the left scatter plot compares the relative ranks induced by our JSS-based mixed proxy (X-axis) and by Hybrid red-teaming scores (Y-axis); points lying near the diagonal blue band indicate close agreement between the two rankings. The right panel in each family shows the corresponding raw JSS-proxy (blue) and Hybrid (red) scores over all subset models, with shaded regions denoting bootstrap variability, again yielding almost identical within-family orderings. Note that "Hybrid" is the overall average across score all tested red-teaming tasks, with detailed task-wise scores provided in Appendix Table 1.

between latent-space dynamics and explicit refusal behavior, establishing an interpretable and measurable indicator of the model’s latent safety awareness.

5.2.3. Conclusion. Overall, we demonstrate that a model’s safety is manifested not only in its observable output content, but more fundamentally in the organization and evolution of its latent representation trajectories under our method. Therefore, analyzing these trajectory’s separability can equally reveal the core safety mechanisms that traditional output-based evaluations seek to capture.

5.3. Model Differentiation and Safety Characterization

This section presents the core capability of our evaluation framework: its ability to precisely and transferably characterize safety differences across models. In other words, the JSS-based system not only captures the internal representational dynamics of a model but also enables multi-scale and fine-grained quantification of safety variation and underlying regularities across different alignment levels. Within this overarching framework, our analyses proceed along two complementary axes:

- **Inter-Model Dimension (Model-Level Differentiation):** examining subtle variations in latent-space

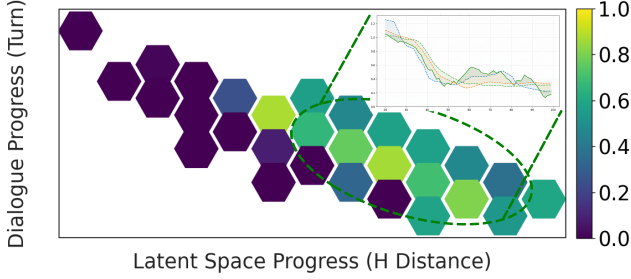


Figure 4: **Coupled dynamics of JSS and ANM along the jailbreak process.** The color indicates the normalized refusal-intensity score (ANM); The inset line plot in the upper-right overlays slice-wise JSS and ANM curves over the standardized progress axis, revealing a shared mid-phase rise and late-phase collapse, which highlights the strong correlation between geometric separability (JSS) and probability-level refusal tendency (ANM).

separability among instruction-aligned models to reveal the continuous distribution of intermediate safety regimes;

- Intra-Model Dimension (Weight-Level Evolution): contrasting forward DPO and inverse DPO settings to observe how safety alignment evolves directionally with changes in alignment weight.

Together, these two perspectives form a progressive precision hierarchy: from inter-model to intra-model analysis—demonstrating that the JSS framework consistently reflects alignment strength across granularities, achieving a unified, continuous, and model-invariant scale for safety evaluation.

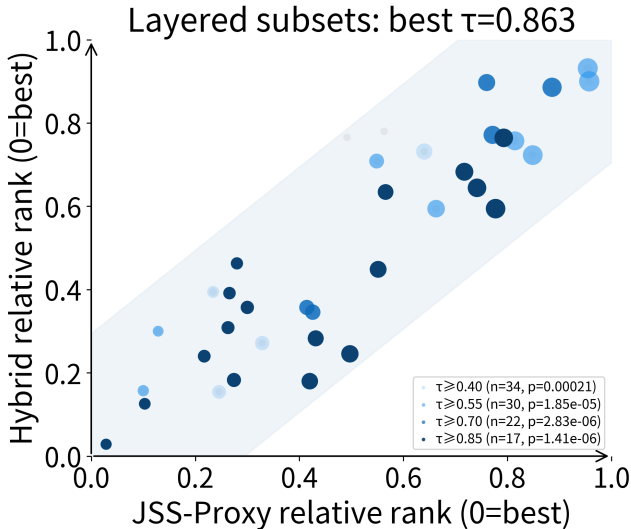


Figure 5: **Layered subset rank consistency with statistically significant (bottom right) agreement across all τ thresholds.**

5.3.1. Cross-Model Validation of JSS-Derived Safety Proxies.

For model-level differentiation, we collected a diverse set of models and evaluated their performance under a series of standardized red-teaming safety tests (21 testing protocols with over 7000 test cases). For each model, the results were aggregated into a single averaged safety score (Hybrid Score). Our goal in this experiment is twofold: (1) to derive proxy safety indicators from our JSS-based evaluation framework, and (2) to assess the consistency between the proxy-based ranking and the ranking obtained from conventional red-teaming safety evaluations.

Building upon the JSS evaluation indices defined earlier, we construct two higher-level proxy metrics that capture complementary aspects of safety separability.

$$\text{JB/PB Ratio} = \frac{\sum_{s \in [0,1]} \text{JSS}_s(\text{J}, \text{B})}{\sum_{s \in [0,1]} \text{JSS}_s(\text{P}, \text{B})} \quad (27)$$

A higher value indicates that the overall separation strength between Jailbreak and Baseline trajectories is significant based on the metric that between PlainQuery and Baseline. This reflects stronger discriminability of jailbreak trajectories.

$$\text{JR Min/Max} = \frac{\min_{s \in [0,1]} \text{JSS}_s(\text{J}, \text{R})}{\max_{s \in [0,1]} \text{JSS}_s(\text{J}, \text{R})} \quad (28)$$

A higher ratio indicates that the Ideal Refusal-Jialbreak separability remains stable across the entire trajectory. If the separation persists throughout decoding, the minimum approaches the maximum, resulting in a higher ratio. Conversely, if the separation collapses near the end—implying successful jailbreak intrusion and erosion of refusal—this ratio drops sharply, capturing the characteristic “mid-phase emergence—end-phase collapse” dynamics. To obtain a unified scalar JSS-proxy for safety alignment evaluation, we combine the two secondary metrics with equal weighting:

$$\text{JSS-Proxy} = 0.5 * \text{JB/PB Ratio} + 0.5 * \text{JR Min/Max}. \quad (29)$$

We quantify the agreement between our proxy-based safety ranking $r_{\text{jss-proxy}}$ and the ranking obtained from conventional red-teaming evaluations r_{Hybrid} using Kendall’s τ correlation coefficient:

$$\tau(r_{\text{jss-proxy}}, r_{\text{Hybrid}}) \in [-1, 1]. \quad (30)$$

Figure 5 and 3 show that cross a sufficiently large model set, the proxy-based ranking exhibits strong concordance with the red-teaming ground truth. This demonstrates that our JSS-derived proxy indicators can accurately reproduce traditional safety orderings within representative alignment regimes, while requiring far lower evaluation cost. As the model pool expands, τ shows a mild decrease but remains consistently high, with p -values far below conventional significance thresholds. This indicates that even under broader model coverage, the alignment between the proxy-based and red-teaming rankings remains statistically significant. Such behavior illustrates the robust hierarchical consistency of our proxy system, maintaining statistically significant agreement

at scale while achieving near-perfect correspondence within focused model subsets.

5.3.2. Consistency under Model Weight Variations. In essence, we demonstrate that the geometric safety scale captured by JSS not only reflects static differences among models but also dynamically responds to behavioral transitions induced by weight adjustments. Specifically, we introduce two opposite preference directions: Forward DPO and Inverse DPO, which respectively correspond to the enhancement and attenuation of safety alignment. We employ the preference optimization loss to fine-tune the same base model in two opposite directions:

$$\mathcal{L}_{\text{DPO}}(\theta) = -\mathbb{E}_{(x, y^+, y^-) \sim \mathcal{D}} \left[\log \sigma(\beta \Delta_\theta) \right] \quad (31)$$

where $\Delta_\theta = \log p_\theta(y^+ | x) - \log p_\theta(y^- | x)$. Specifically, we deploy it for two purposes:

Forward DPO. The model is fine-tuned with safety-oriented preferences, where compliant responses are favored over harmful ones ($y^+ = \text{safe}$, $y^- = \text{harmful}$).

Inverse DPO. We reverse the preference direction so that harmful responses are favored over compliant ones ($y^+ = \text{harmful}$, $y^- = \text{safe}$).

To avoid conclusions biased by a single fine-tuning intensity, we systematically generate a structured set of model variants within the LoRA parameter space, fixing the base model and dataset while varying: LoRA target modules and LoRA Rank.

Figure 6 illustrates that from a correlation perspective, the local peaks and troughs of the JSS curves strongly align with fluctuations in the surface safety metrics, including both Unsafe Rate and Refusal Rate (Definition in Appendix Section A). This observation indicates that the degree of separability in latent space evolves in synchrony with the model’s explicit refusal behaviors in output space.

A closer examination reveals a consistent time lag of several training windows between the changes in JSS and the corresponding shifts in surface metrics, with the effect being particularly evident in the early stages of Inverse DPO. Quantitatively, the lag is strongest under Inverse DPO (about 76% of runs exhibit lag). For Forward DPO, in the RefEx–JB family, 74% of trajectories show “JSS leads, refusal lags,” with a median shift of -4.4 steps, whereas in JB–Baseline the effect weakens but persists (64%, median -1.4). For the unsafe rate, both families show near-synchronous behavior (RefEx–JB: 45% lead / 48% lag; JB–Baseline centered around zero with median -0.6).

Together, these results show that declines in latent-space separability reliably precede the corresponding drops in observable safety behaviors—typically by several training windows—establishing JSS as a robust early-warning signal for impending safety degradation during training.

To complement the dual-line analysis, we compute Pearson and Spearman correlations between latent JSS signals and surface safety metrics across lower, middle, and upper layers (Figure 7). As shown in the heatmaps, the correlation signs are fully consistent across all layer groups and

both alignment directions. This confirms that JSS reliably tracks the direction of safety strengthening or weakening, providing a stable latent–surface correspondence.

5.4. Baseline Comparison: Cost and Efficiency of Traditional Red-Teaming vs. Our JSS-Only Pipeline

The goal of this experiment is to quantitatively compare resource consumption of two assessment pipelines under identical task scale and sample size conditions:

- **Ours.** Representation-based evaluation using offline attack trajectories. We execute a single forward pass on the subject model M_s to extract hidden states; no online generation or additional evaluator inference is required.
- **Baseline (traditional online red-team + llm-based evaluator).** We run online red-teaming and safety evaluation using a PyRIT + Ollama setup, involving three model roles:
 - M_r : red-team attack generator,
 - M_s : subject model under test,
 - M_e : evaluator / safety discriminator.

Denote the total number of attack targets by N , the average number of turns per session by \bar{T} , and the average tokens per step by \bar{L} . We formalize token and time costs for both pipelines as follows.

For our method, only a forward pass per turn of offline attack dataset on M_s is required and hidden states are cached, then we can get the token cost and runtime cost:

$$C_{\text{token}}^{\text{Ours}}(N) = N \cdot \bar{T}_{\text{offline}}, \quad (32)$$

$$C_{\text{time}}^{\text{Ours}} = \text{Time}_{M_s^{\text{forward}}} + \text{Time}_{\text{offline_JSS}} + \text{Time}_{\text{benign_con}}, \quad (33)$$

where $\text{Time}_{M_s^{\text{forward}}}$ denotes the cost of $C_{\text{token}}^{\text{Ours}}(N, J)$, $\text{Time}_{\text{offline_JSS}}$ denotes the downstream cost for JSS statistics, and $\text{Time}_{\text{benign_con}}$ denotes time to construct the benign distribution (both $\text{Time}_{\text{benign_con}}$ and $\text{Time}_{\text{offline_JSS}}$ are typically much smaller than generation time, so we ignore them in following analysis).

For traditional baseline, each red-team attempt involves a three-way inference flow for T attack turns and N attack targets:

$$C_{\text{token}}^{\text{Base}}(N) = N \cdot \bar{T}_r \cdot (\bar{L}_r + \bar{L}_s + \bar{L}_e), \quad (34)$$

$$C_{\text{time}}^{\text{Base}} = \text{Time}_{M_r} + \text{Time}_{M_s} + \text{Time}_{M_e}, \quad (35)$$

where $\bar{L}_r, \bar{L}_s, \bar{L}_e$ denote the average token lengths for red-team generation, subject-model generation, and evaluator judgment respectively. \bar{T}_r denotes the average turn number of attacks generated by redteaming models.

We run evaluations at multiple red-team intensities $N = \{n_1, n_2, \dots\}$ using PyRIT’s redteaming module to generate online attacks, and record produced token counts and elapsed times. For the JSS method, we count a single forward pass per example as one token-equivalent

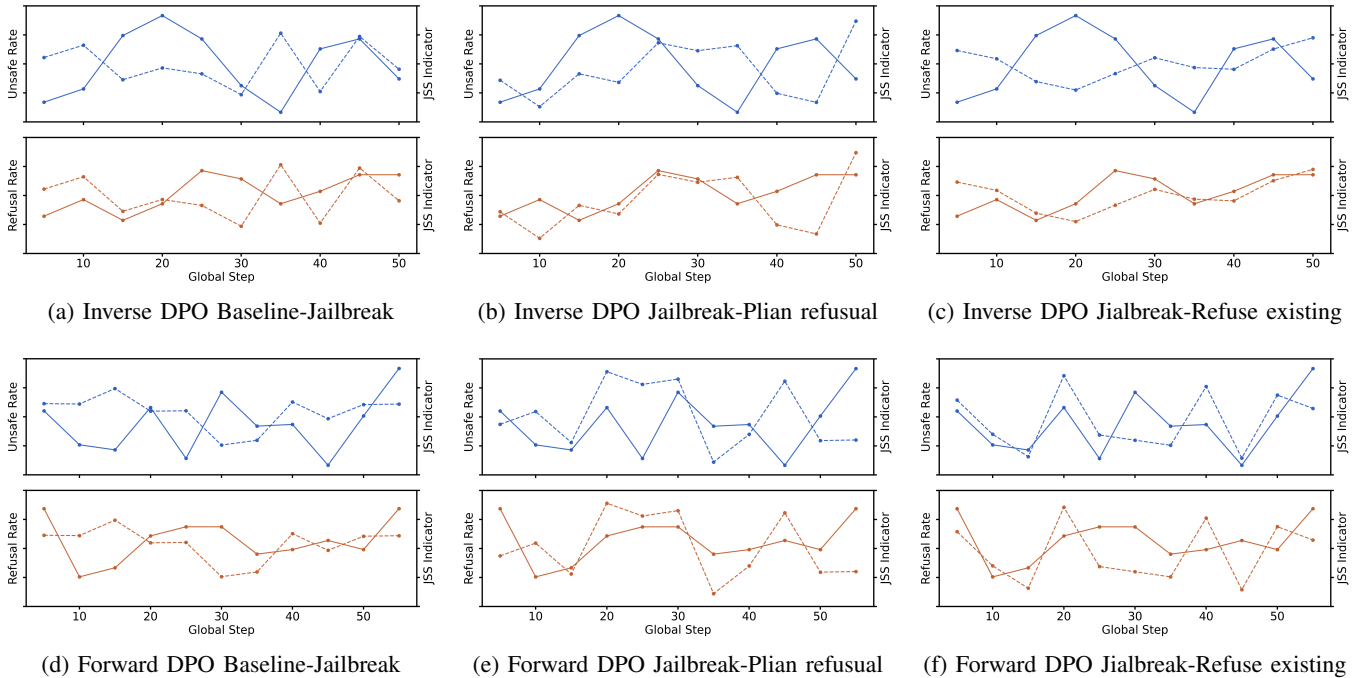


Figure 6: **Evolution of JSS and behavioral safety metrics under Forward vs. Inverse DPO.** The dynamic evolution of both surface-level safety behavior metrics (solid lines: unsafe rate and refusal rate) and latent proxy metrics (dashed lines: JSS) as functions of the training global step during the Forward DPO (lower row) and Inverse DPO (upper row) processes. The three columns respectively correspond to separability relations across different dialogue families.

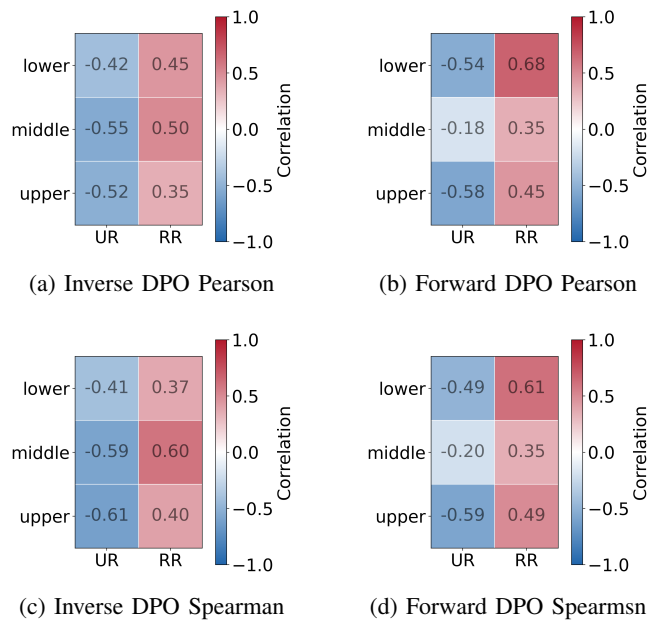


Figure 7: **Safety Metrics (UR: Unsafe Rate; RR: Refusal Rate) and JSS Correlation Heatmap**

for bookkeeping; the JSS evaluation uses the same original instruction set N corresponding offline multi-turn jailbreak datasets, derived RefEx and PlainR sets. We record token-equivalent costs and elapsed wall-clock time for both pipelines.

We compare the two pipelines along the following axes:

- **Relative share of output tokens:** the fraction of total system tokens generated by the subject model M_s during evaluation.
- **Total generated-token count:** the overall number of tokens produced by all system components during evaluation.
- **Per-token time cost:** wall-clock runtime divided by total produced tokens; this metric measures system throughput. Lower per-token time denotes higher efficiency.

Figure 8 summarizes the cost comparison across all metrics, all roles, and all red-teaming depths, the JSS-only pipeline remains dramatically—often orders of magnitude—more efficient than the traditional three-model setup.

Together, these three findings establish that N-GLARE reduces evaluation cost by at least two orders of magnitude while preserving ranking fidelity, effectively removing the generative bottleneck that makes traditional red-teaming expensive, slow, and difficult to scale.

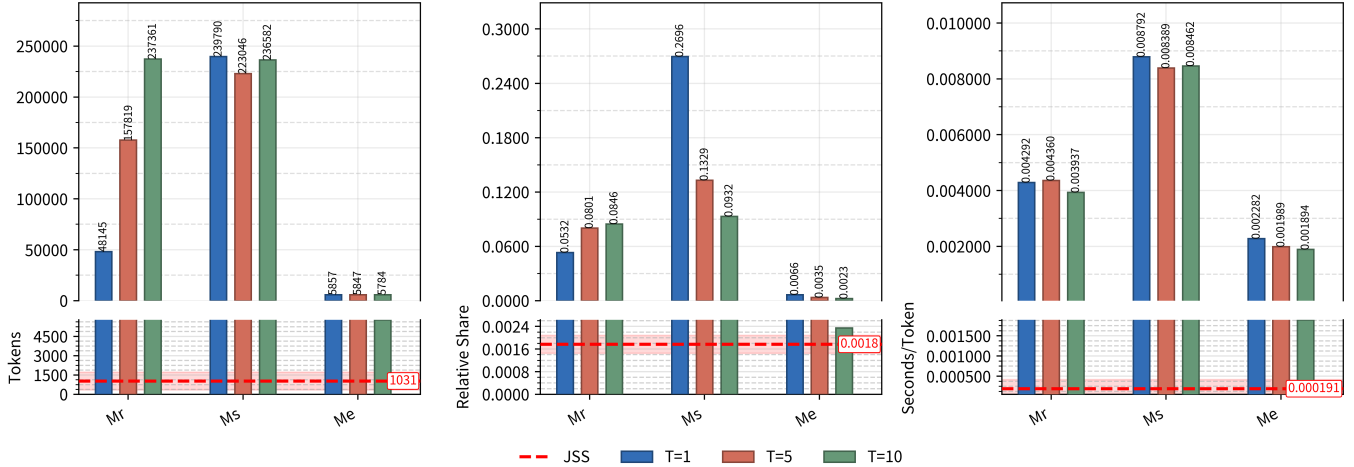
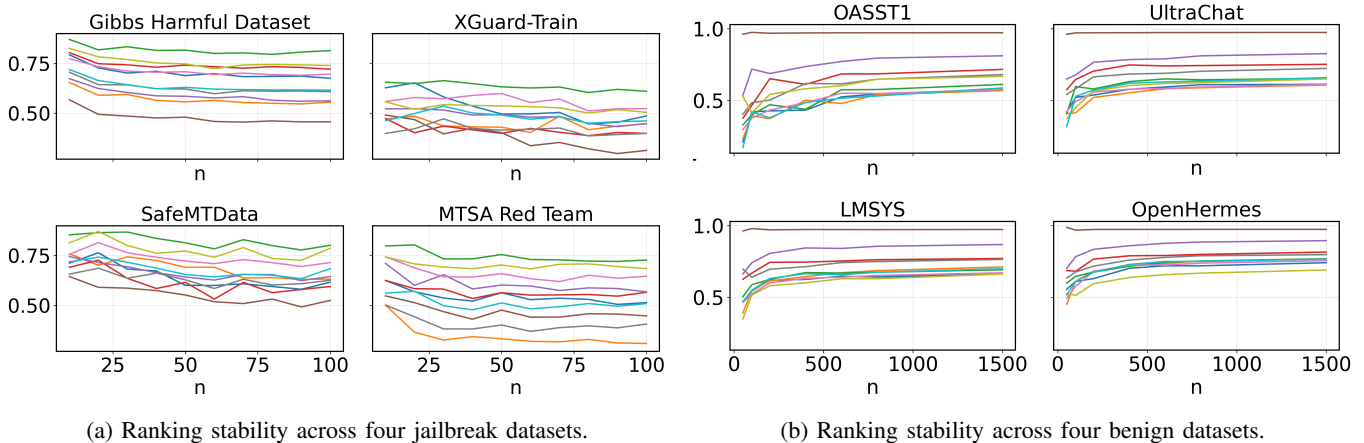


Figure 8: **Comparative cost breakdown of traditional three-model red-teaming versus our JSS-only pipeline.** For increasing red-teaming depths ($T = 1, 5, 10$), the three panels report (left) total generated tokens, (middle) the relative share produced by each role—attacker (M_r), subject model (M_s), evaluator (M_e)—and (right) the per-token runtime cost.



(a) Ranking stability across four jailbreak datasets.

(b) Ranking stability across four benign datasets.

Figure 9: **Stability of normalized JSS-induced ranking value under varying sample sizes across jailbreak and benign datasets.** Across all settings, the curves remain smooth and largely monotonic, confirming that N-GLARE yields stable safety ordering even when trajectory sampling budgets are perturbed.

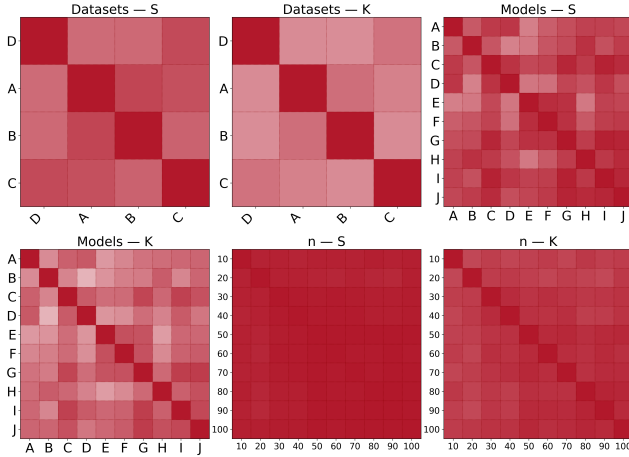
5.5. Model Sensitivity and Systemic Stability Experiments

If our method is indeed capturing an intrinsic property of the model’s alignment dynamics—rather than dataset-specific artifacts—then its induced safety ordering should remain stable when we perturb the underlying data and sampling conditions. The goal of this section is therefore to test the *systemic stability* of our JSS-based safety scale. Concretely, we ask:

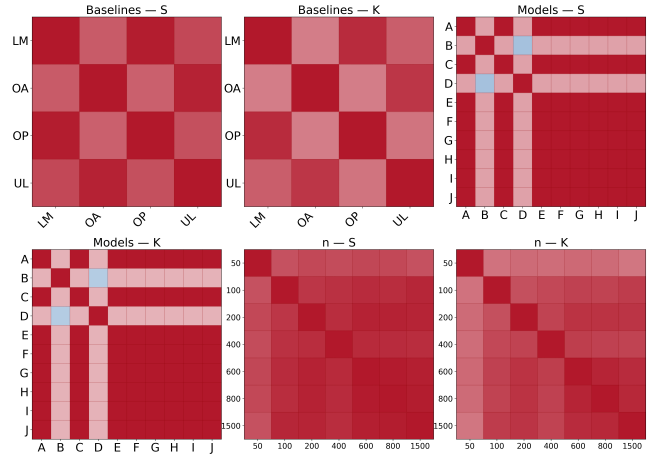
- whether the relative JSS differences between models (i.e., the safety ranking induced by JSS) remain consistent when we vary which jailbreak trajectories are used under different attack datasets and how many sample size n trajectories are included; and

- whether the same stability holds when we perturb the benign reference distribution, by changing the source corpus and the number of benign samples used to estimate the natural manifold.

To assess whether JSS captures a dataset-agnostic and sample-size-agnostic property of model alignment dynamics, we evaluate stability under both jailbreak and benign perturbations. For jailbreak analysis, we use four multi-turn attack datasets—(D)=tom-gibbs, (A)=XGuard-Train, (B)=SafeMTData, (C)=MTSARed—and vary the number of included targets to produce small/medium/large (n)-sample conditions (each yielding $(5-10 \times n)$ activation trajectories). Figure 10 shows that across all settings, JSS-induced rankings remain highly consistent: Dataset–Dataset correlations reach mean Spearman (0.7150) and Kendall (0.5411); Model–Model comparisons show stable ordering;



(a) Sensitivity analysis on jailbreak datasets.



(b) Sensitivity analysis on benign datasets.

Figure 10: **Sensitivity heatmaps for JSS-based ranking across datasets, models (see Appendix Table 3 for alphabetical labels mapping), baselines, and sample sizes.** Each heatmap visualizes pairwise rank consistency between two evaluation settings computed with two rank correlation metrics (S = Spearman, K = Kendall), where darker cells indicate higher agreement. Rows and columns correspond to jailbreak datasets, models, baseline datasets, or sampling budgets n .

and varying (n) preserves strong agreement (mean Spearman (0.7973), Kendall (0.6328)). Even in pairwise ($n \times n$) evaluations, consistency remains extremely high (Spearman (0.9691), Kendall (0.8677)). An identical analysis on benign-distribution estimation—using four instruction-following corpora (LM)=LMSYS, (OA)=OASST1, (OP)=OpenHermes, (UL)=UltraChat—shows similarly robust behavior, with Dataset–Dataset correlations (mean Spearman (0.7012), Kendall (0.5237)) and Model–Model comparisons both remaining stable, and sample-size variation maintaining strong consistency (mean Spearman (0.81), Kendall (0.61)). Finally, Figure 9 provides a more intuitive visualization: as (n) increases, normalized JSS ranking curves across all jailbreak and benign datasets evolve smoothly and converge without reversals, reinforcing that JSS-based safety ordering is structurally stable across datasets, models, and sampling budgets.

6. Conclusion

This paper introduces N-GLARE, a non-generative, representation-based framework for LLM safety evaluation, showing that a model’s safety state is encoded not only in its outputs but in the geometry and dynamics of its latent trajectories. By constructing a benign distribution manifold and using JSS to quantify how jailbreak and ideal-refusal trajectories deviate from it, we obtain safety indicators that are comparable across models. Across more than 40 models and multiple red-teaming strategies, N-GLARE’s safety rankings remain consistent with large-scale red-teaming evaluations while reducing evaluation cost by over two orders of magnitude. Beyond reproducing traditional benchmarks, N-GLARE uncovers finer-grained safety dynamics, such as the phase structure of jailbreak progression, the synchronized evolution of refusal tendency, and monotonic

trends under forward and inverse DPO, showcasing latent-trajectory analysis as a scalable paradigm for model-level safety diagnostics and providing a new foundation for continuous alignment monitoring and future alignment research.

References

- [1] A. Grattafiori, A. Dubey, A. Jauhri, A. Pandey, A. Kadian, A. Al-Dahle, A. Letman, A. Mathur, A. Schelten, A. Vaughan *et al.*, “The llama 3 herd of models,” *arXiv preprint arXiv:2407.21783*, 2024.
- [2] H. Zhou, C. Hu, Y. Yuan, Y. Cui, Y. Jin, C. Chen, H. Wu, D. Yuan, L. Jiang, D. Wu *et al.*, “Large language model (llm) for telecommunications: A comprehensive survey on principles, key techniques, and opportunities,” *IEEE Communications Surveys & Tutorials*, vol. 27, no. 3, pp. 1955–2005, 2024.
- [3] B. C. Das, M. H. Amini, and Y. Wu, “Security and privacy challenges of large language models: A survey,” *ACM Computing Surveys*, vol. 57, no. 6, pp. 1–39, 2025.
- [4] Z. Dong, Z. Zhou, C. Yang, J. Shao, and Y. Qiao, “Attacks, defenses and evaluations for llm conversation safety: A survey,” *arXiv preprint arXiv:2402.09283*, 2024.
- [5] A. Wei, N. Haghtalab, and J. Steinhardt, “Jailbroken: How does llm safety training fail?” *Advances in Neural Information Processing Systems*, vol. 36, pp. 80 079–80 110, 2023.
- [6] M. Russinovich, A. Salem, and R. Eldan, “Great, now write an article about that: The crescendo {Multi-Turn}{LLM} jailbreak attack,” in *34th USENIX Security Symposium (USENIX Security 25)*, 2025, pp. 2421–2440.
- [7] J. Yang, Z. Lin, S. Yang, Z. Lu, and X. Du, “Concept enhancement engineering: A lightweight and efficient robust defense against jailbreak attacks in embodied ai,” *arXiv preprint arXiv:2504.13201*, 2025.
- [8] L. Lin, H. Mu, Z. Zhai, M. Wang, Y. Wang, R. Wang, J. Gao, Y. Zhang, W. Che, T. Baldwin *et al.*, “Against the achilles’ heel: A survey on red teaming for generative models,” *Journal of Artificial Intelligence Research*, vol. 82, pp. 687–775, 2025.
- [9] A. Zou, L. Phan, S. Chen, J. Campbell, P. Guo, R. Ren, A. Pan, X. Yin, M. Mazeika, A.-K. Dombrowski *et al.*, “Representation engineering: A top-down approach to ai transparency,” *arXiv preprint arXiv:2310.01405*, 2023.

- [10] T. Li, Z. Wang, W. Liu, M. Wu, S. Dou, C. Lv, X. Wang, X. Zheng, and X.-J. Huang, "Revisiting jailbreaking for large language models: A representation engineering perspective," in *Proceedings of the 31st International Conference on Computational Linguistics*, 2025, pp. 3158–3178.
- [11] T. Cui, Y. Wang, C. Fu, Y. Xiao, S. Li, X. Deng, Y. Liu, Q. Zhang, Z. Qiu, P. Li, Z. Tan, J. Xiong, X. Kong, Z. Wen, K. Xu, and Q. Li, "Risk taxonomy, mitigation, and assessment benchmarks of large language model systems," *ArXiv*, vol. abs/2401.05778, 2024.
- [12] K. Zhu, J. Wang, J. Zhou, Z. Wang, H. Chen, Y. Wang, L. Yang, W. Ye, Y. Zhang, N. Zhenqiang Gong *et al.*, "Promptbench: Towards evaluating the robustness of large language models on adversarial prompts," *arXiv e-prints*, pp. arXiv–2306, 2023.
- [13] A. Paulus, A. Zharmagambetov, C. Guo, B. Amos, and Y. Tian, "Advprompter: Fast adaptive adversarial prompting for llms," *arXiv preprint arXiv:2404.16873*, 2024.
- [14] E. A. Oliveira, M. Mohoni, S. López-Pernas, and M. Saqr, "Human-ai collaboration or academic misconduct? measuring ai use in student writing through stylometric evidence," *arXiv preprint arXiv:2505.08828*, 2025.
- [15] J. Xu, J. W. Stokes, G. McDonald, X. Bai, D. Marshall, S. Wang, A. Swaminathan, and Z. Li, "Autoattacker: A large language model guided system to implement automatic cyber-attacks," *arXiv preprint arXiv:2403.01038*, 2024.
- [16] J. Xu, S. Li, Z. Xu, and D. Zhang, "Do llms know to respect copyright notice?" *arXiv preprint arXiv:2411.01136*, 2024.
- [17] V. S. Sadasivan, S. Saha, G. Sriramanan, P. Kattakinda, A. Chegini, and S. Feizi, "Fast adversarial attacks on language models in one gpu minute," *arXiv preprint arXiv:2402.15570*, 2024.
- [18] J. Yu, X. Lin, Z. Yu, and X. Xing, "Gptfuzzer: Red teaming large language models with auto-generated jailbreak prompts," *arXiv preprint arXiv:2309.10253*, 2023.
- [19] S. Rahman, L. Jiang, J. Shiffer, G. Liu, S. Issaka, M. R. Parvez, H. Palangi, K.-W. Chang, Y. Choi, and S. Gabriel, "X-teaming: Multi-turn jailbreaks and defenses with adaptive multi-agents," *arXiv preprint arXiv:2504.13203*, 2025.
- [20] Z. Weng, X. Jin, J. Jia, and X. Zhang, "Foot-in-the-door: A multi-turn jailbreak for llms," *arXiv preprint arXiv:2502.19820*, 2025.
- [21] Q. Ren, H. Li, D. Liu, Z. Xie, X. Lu, Y. Qiao, L. Sha, J. Yan, L. Ma, and J. Shao, "Llms know their vulnerabilities: Uncover safety gaps through natural distribution shifts," in *Proceedings of the 63rd Annual Meeting of the Association for Computational Linguistics (Volume 1: Long Papers)*, 2025, pp. 24 763–24 785.
- [22] A. Rogers, O. Kovaleva, and A. Rumshisky, "A primer in bertology: What we know about how bert works," *Transactions of the association for computational linguistics*, vol. 8, pp. 842–866, 2020.
- [23] J. Lee, W. Yoon, S. Kim, D. Kim, S. Kim, C. H. So, and J. Kang, "Biobert: a pre-trained biomedical language representation model for biomedical text mining," *Bioinformatics*, vol. 36, no. 4, pp. 1234–1240, 2020.
- [24] I. Tenney, D. Das, and E. Pavlick, "Bert rediscovers the classical nlp pipeline," *arXiv preprint arXiv:1905.05950*, 2019.
- [25] M. Cai, Y. Zhang, S. Zhang, F. Yin, D. Zhang, D. Zou, Y. Yue, and Z. Hu, "Self-control of llm behaviors by compressing suffix gradient into prefix controller," *arXiv preprint arXiv:2406.02721*, 2024.
- [26] H. Wang, Y. Yue, R. Lu, J. Shi, A. Zhao, S. Wang, S. Song, and G. Huang, "Model surgery: Modulating llm's behavior via simple parameter editing," in *Proceedings of the 2025 Conference of the Nations of the Americas Chapter of the Association for Computational Linguistics: Human Language Technologies (Volume 1: Long Papers)*, 2025, pp. 6337–6357.
- [27] P. Wang, D. Zhang, L. Li, C. Tan, X. Wang, M. Zhang, K. Ren, B. Jiang, and X. Qiu, "Inferaligner: Inference-time alignment for harmlessness through cross-model guidance," in *Proceedings of the 2024 Conference on Empirical Methods in Natural Language Processing*, 2024, pp. 10 460–10 479.
- [28] Z. Cao, Y. Yang, and H. Zhao, "Nothing in excess: Mitigating the exaggerated safety for llms via safety-conscious activation steering," *arXiv e-prints*, pp. arXiv–2408, 2024.
- [29] S. Marks and M. Tegmark, "The geometry of truth: Emergent linear structure in large language model representations of true/false datasets," *arXiv preprint arXiv:2310.06824*, 2023.
- [30] K. Li, O. Patel, F. Viégas, H. Pfister, and M. Wattenberg, "Inference-time intervention: Eliciting truthful answers from a language model," *Advances in Neural Information Processing Systems*, vol. 36, pp. 41 451–41 530, 2023.
- [31] T. Wang, X. Jiao, Y. Zhu, Z. Chen, Y. He, X. Chu, J. Gao, Y. Wang, and L. Ma, "Adaptive activation steering: A tuning-free llm truthfulness improvement method for diverse hallucinations categories," in *Proceedings of the ACM on Web Conference 2025*, 2025, pp. 2562–2578.
- [32] N. Rimskey, N. Gabrieli, J. Schulz, M. Tong, E. Hubinger, and A. Turner, "Steering llama 2 via contrastive activation addition," in *Proceedings of the 62nd Annual Meeting of the Association for Computational Linguistics (Volume 1: Long Papers)*, 2024, pp. 15 504–15 522.
- [33] A. Ardití, O. Obeso, A. Syed, D. Paleka, N. Panickssery, W. Gurnee, and N. Nanda, "Refusal in language models is mediated by a single direction," *Advances in Neural Information Processing Systems*, vol. 37, pp. 136 037–136 083, 2024.
- [34] J. Vig, "A multiscale visualization of attention in the transformer model," *arXiv preprint arXiv:1906.05714*, 2019.
- [35] P. Michel, O. Levy, and G. Neubig, "Are sixteen heads really better than one?" *Advances in neural information processing systems*, vol. 32, 2019.
- [36] A. Jaegle, F. Gimeno, A. Brock, O. Vinyals, A. Zisserman, and J. Carreira, "Perceiver: General perception with iterative attention," in *International conference on machine learning*. PMLR, 2021, pp. 4651–4664.
- [37] J. Wei, X. Wang, D. Schuurmans, M. Bosma, F. Xia, E. Chi, Q. V. Le, D. Zhou *et al.*, "Chain-of-thought prompting elicits reasoning in large language models," *Advances in neural information processing systems*, vol. 35, pp. 24 824–24 837, 2022.
- [38] H. Li, S. Bai, J. Zhang, and S. Guo, "Core: Enhancing metacognition with label-free self-evaluation in llms," *arXiv preprint arXiv:2507.06087*, 2025.
- [39] C. Eckart and G. Young, "The approximation of one matrix by another of lower rank," *Psychometrika*, vol. 1, no. 3, pp. 211–218, 1936.
- [40] G. H. Golub and C. F. Van Loan, *Matrix Computations*, 4th ed. Johns Hopkins University Press, 2013.
- [41] M. P. do Carmo, *Differential Geometry of Curves and Surfaces*. Prentice-Hall, 1976.
- [42] T. Hastie, R. Tibshirani, and J. Friedman, *The Elements of Statistical Learning: Data Mining, Inference, and Prediction*, 2nd ed. Springer, 2009.

Appendix

Table 1 presents the performance of 36 large language models tested across various security evaluation tasks. These tasks primarily measure their ability to resist jailbreak attacks, bypass protective mechanisms, and handle harmful instructions. The data in the table includes the models' effectiveness in rejecting malicious requests, their ability to defend against bypass attacks, and their vulnerabilities in specific tasks such as ASCII art interpretation exploits and role-playing attacks.

TABLE 1: Model Safety Benchmark Results

models	JB/RE↑	BJ/BP↑	AI Safety↑	None	ABJ	Adaptive	ArtPrompt	AutoDAN	Cipher	DAN	DeepInc	DevMode	DRA	DrAttack	GCG	GPTFuzzer	Grandmother	Masterkey	MultiLing	PAIR	PastTense	Psychology	ReNeLLM	TAP
1 Llama-3.2-3B-Instruct	0.6733	0.2899	81.89	91.18	83.62	44.42	47.31	97.85	100	99.57	94.40	96.12	94.05	91.38	95.72	90.95	97.71	98.28	78.83	97.41	100	95.69	64.08	98.28
2 Qwen/Qwen2.5-7B-Instruct	0.5346	0.4414	55.17	97.78	17.42	13.82	50.28	56.94	28.93	95.26	42.81	96.88	8.29	33.69	86.80	33.16	90.24	98.63	95.09	86.51	99.52	93.10	33.91	84.74
3 mistralai/Mistral-7B-Instruct-v0.3	0.3582	0.1776	34.69	61.03	8.12	6.03	25.53	47.01	3.45	20.26	25.43	23.71	2.05	31.19	37.87	23.62	70.69	71.55	63.12	79.05	84.05	80.60	23.41	78.02
4 Llama-3.1-8B-it	0.4312	0.2538	93.22	100	99.14	65.38	100	98.71	99.43	99.14	97.63	100	97.43	89.66	99.57	95.30	98.28	100	93.63	97.41	98.71	100	90.52	100
5 google/gemma-7b-it	0.6992	0.5768	64.02	94.50	56.03	36.85	48.08	69.83	100	72.41	38.36	97.86	19.86	71.92	90.95	64.39	96.12	90.95	69.26	80.60	97.84	96.12	29.70	90.09
6 Mistral-7B-Instruct-v0.2	0.3400	0.3526	36.92	40.20	7.66	4.77	54.74	42.49	6.03	12.07	19.83	24.57	1.49	40.73	29.13	32.61	63.52	78.02	60.25	65.95	97.41	79.74	32.62	67.38
7 nvidia/Nemotron-Mini-4B-Instruct	0.5784	0.3118	51.57	96.85	22.83	12.54	95.28	50.00	99.21	29.13	35.43	91.49	7.31	38.12	93.97	33.00	85.83	99.21	92.13	82.68	96.06	74.02	23.08	75.00
8 Baichuan2-7B-Chat	0.2792	0.5432	33.17	46.17	35.04	11.50	13.79	35.97	20.16	13.96	10.84	37.72	10.03	11.74	23.35	45.94	71.80	47.86	58.18	74.25	84.05	72.33	24.07	62.12
9 gemma-2-9b-it	0.3329	0.4727	67.63	95.62	68.10	2.15	89.22	78.02	25.00	25.43	64.67	53.45	31.21	93.10	96.99	24.35	85.34	100	100	89.66	100	99.57	78.02	92.27
10 TinySwallow-1.5B-Instruct	0.6708	0.3339	68.22	98.43	44.88	14.76	98.43	71.65	100	94.49	44.88	100	46.13	63.24	98.43	57.43	96.06	98.43	97.64	86.61	100	98.43	57.14	92.13
11 microsoft/Phi-3-mini-4k-instruct	0.2995	0.5432	63.90	96.05	78.74	21.09	92.91	74.80	97.64	99.21	37.80	99.21	11.49	33.89	96.85	61.72	87.40	100	68.04	88.19	100	97.64	57.98	88.19
12 google/gemma-3-12b-it	0.6629	0.3645	71.16	98.45	85.83	18.11	85.04	90.55	21.71	88.28	88.19	86.99	10.51	64.66	96.85	63.79	88.98	97.64	100	95.28	100	96.85	67.50	96.85
13 Llama-3.1-Tulu-3-8B	0.9034	0.2734	65.95	96.26	32.81	43.19	49.68	62.89	96.25	100	38.58	98.43	10.79	56.41	88.75	73.97	100	100	90.55	100	100	100	65.54	100
14 granite-3.0-8b-instruct	0.4594	0.5180	61.30	99.63	27.59	58.79	28.63	63.39	55.17	89.37	15.19	91.81	12.89	36.07	98.71	60.83	99.14	99.14	78.15	91.81	99.14	98.71	61.55	86.21
15 DeepSeek-R1-Distill-Qwen-7B	0.5685	1.0285	53.49	65.73	25.20	28.38	82.67	75.78	26.77	83.43	64.84	83.12	33.90	49.57	44.09	89.06	59.68	54.33	58.24	87.58	33.49	77.17	42.23	87.64
16 microsoft/Phi-3-mini-128k-instruct	0.2784	0.4763	53.82	94.87	30.60	6.78	84.48	71.98	80.17	95.69	21.98	97.41	5.38	26.61	93.58	47.65	80.60	100	67.42	84.48	100	94.86	44.63	80.76
17 Mistral-NeMo-Minitron-8B-Instruct	0.7369	0.3435	47.88	84.85	19.69	21.76	35.55	48.41	14.61	43.51	29.69	36.32	3.75	43.34	91.34	36.12	90.55	86.87	74.72	87.49	96.06	81.38	59.08	71.79
18 01-ai/Yi-1.5-9B-Chat	0.1992	0.7507	39.36	85.17	12.93	3.39	39.24	61.64	27.35	9.83	21.98	53.06	11.75	23.60	67.95	27.14	74.68	86.18	47.63	77.34	93.10	75.54	27.04	76.82
19 Yi-6B-Chat	0.5100	0.3796	43.36	46.25	9.32	8.78	36.01	42.34	60.51	73.18	13.26	80.69	4.87	69.47	74.88	31.84	81.33	94.40	61.35	72.10	97.84	92.24	23.35	67.72
20 Qwen/Qwen2.5-0.5B-Instruct	0.5723	0.1777	44.05	75.06	11.71	4.45	59.99	48.15	93.13	47.45	23.24	92.67	12.81	32.20	61.16	38.57	80.76	67.81	86.92	76.76	98.28	61.45	23.84	66.08
21 Qwen2.5-1.5B-Instruct	0.6726	0.3052	52.40	98.90	11.82	17.69	85.34	48.29	99.14	72.75	29.23	97.43	14.29	23.51	87.17	43.02	95.69	95.69	91.10	81.03	99.14	85.78	21.97	76.06
22 Qwen2.5-14B-Instruct	0.4591	0.4041	68.61	99.63	28.80	4.27	91.38	83.19	78.45	98.28	58.80	98.28	36.62	58.19	93.60	67.38	96.55	100	100	94.83	96.12	99.14	77.59	92.67
23 google/gemma-3-4b-it	0.4624	0.2563	57.75	93.87	50.39	11.81	56.69	75.59	17.97	42.18	69.29	39.37	22.56	49.14	94.53	52.13	66.93	97.64	98.43	91.34	100	98.43	51.26	95.28
24 google/gemma-3-1b-it	0.6095	0.5359	65.19	96.15	59.06	15.50	60.77	73.23	83.46	22.05	70.08	80.60	44.69	41.15	96.85	37.07	71.65	100	96.85	93.70	99.21	94.49	65.55	88.98
25 gemma-2-2b-it	0.2755	0.2885	65.56	72.79	46.12	48.08	85.38	81.03	38.57	23.85	70.93	66.38	32.13	76.55	98.71	19.31	82.33	100	99.57	90.09	66.67	99.57	83.33	90.09
26 DeepSeek-R1-Distill-Qwen-1.5B	0.2589	0.7154	40.60	41.18	19.53	30.10	61.60	82.36	27.09	31.92	66.89	15.25	17.74	49.94	25.39	38.26	39.14	25.30	44.60	63.69	34.37	49.74	51.52	60.61
27 DeepSeek-R1-Distill-Qwen-14B	0.5352	1.4011	57.53	76.38	34.65	24.22	80.60	75.59	32.81	27.34	70.08	25.20	34.78	65.52	59.06	74.05	74.21	44.09	80.31	84.72	77.07	88.98	63.03	83.20
28 deepseek-ai/DeepSeek-R1-Distill-Llama-8B	0.5352	1.4011	51.17	70.25	21.26	23.26	92.23	61.71	39.84	36.60	49.22	31.25	29.42	53.45	51.97	86.11	69.29	59.84	62.20	86.03	55.35	85.04	39.50	79.42
29 meta-llama/Meta-Llama-3-8B-Instruct	0.0798	0.2441	79.98	91.61	71.12	80.26	72.13	97.84	100	71.37	93.99	100	20.84	83.33	96.57	97.13	93.16	67.24	98.71	98.71	99.57	100	87.60	98.71

Continued on next page

models	JB/RE↑	BJ/BP↑	AI Safety↑	None	ABJ	Adaptive	ArtPrompt	AutoDAN	Cipher	DAN	DeepInc	DevMode	DRA	DrAttack	GCG	GPTFuzzer	Grandmother	Masterkey	MultiLing	PAIR	PastTense	Psychology	ReNeLLM	TAP
30 meta-llama/Llama-2-7b-chat-hf	0.7188	0.4138	64.47	46.79	98.71	7.73	99.14	88.53	100	89.80	47.09	98.71	12.33	73.07	97.41	58.40	91.38	100	76.60	90.09	100	99.14	85.99	88.36
31 meta-llama/Llama-2-13b-chat-hf	0.7386	1.4244	75.40	63.94	98.56	85.46	83.73	80.52	99.71	98.28	59.48	99.43	12.36	60.51	96.57	66.72	99.14	99.57	75.49	91.38	99.57	100	89.66	90.99
32 Qwen/Qwen2.5-72B-Instruct	0.5530	0.6269	79.41	97.71	54.61	10.80	98.86	78.06	100	98.58	88.67	95.74	83.13	61.76	98.29	86.25	95.73	100	98.29	87.75	99.43	98.29	81.63	92.88
33 Qwen/Qwen2.5-32B-Instruct	0.4748	0.5229	68.81	97.10	56.56	12.57	94.17	79.12	44.30	92.87	55.67	97.69	28.12	64.47	96.24	64.71	93.44	99.60	97.81	92.24	100	97.48	70.77	89.43
34 Qwen/Qwen2.5-3B-Instruct	0.3775	0.3692	51.16	98.92	23.10	9.36	36.22	49.57	63.68	81.47	25.64	97.41	11.10	26.18	94.45	28.74	93.10	99.14	91.02	78.11	100	95.26	35.22	80.60
35 meta-llama/Meta-Llama-3-70B-Instruct	0.9358	0.2999	59.43	74.28	93.10	40.14	14.35	92.75	100	96.84	17.28	83.49	51.15	45.19	91.52	83.43	81.52	94.89	68.37	57.77	54.30	94.01	45.48	55.94
36 Llama-3.1-Nemotron-70B-Instruct-HF	0.2293	0.4283	69.69	92.96	32.28	84.15	79.31	75.78	84.37	66.93	54.33	78.74	14.30	60.34	94.83	75.86	95.28	96.06	89.06	94.53	100	98.43	69.23	93.16

TABLE 2: Model–Abbreviation Mapping of Subset models Scatter Figure

Model	Abbr
01-ai/Yi-1.5-9B-Chat	CHA-9B
Baichuan2-7B-Chat	BAI-7B
DeepSeek-R1-Distill-Qwen-1.5B	DEE-1.5B
DeepSeek-R1-Distill-Qwen-14B	DEE-14B
DeepSeek-R1-Distill-Qwen-7B	DEE-7B
Llama-3.1-8B-it	LLA-8B
Llama-3.1-Nemotron-70B-Instruct-HF	LLA-70B
Llama-3.1-Tulu-3-8B	LLA-8B
Llama-3.2-3B-Instruct	LLA-3B
Mistral-7B-Instruct-v0.2	MIS-7B
Mistral-NeMo-Minitron-8B-Instruct	MIS-8B
Qwen/Qwen2.5-0.5B-Instruct	INS-0.5B
Qwen/Qwen2.5-32B-Instruct	INS-32B
Qwen/Qwen2.5-3B-Instruct	INS-3B
Qwen/Qwen2.5-72B-Instruct	INS-72B
Qwen/Qwen2.5-7B-Instruct	INS-7B
Qwen2.5-1.5B-Instruct	QWE-1.5B
Qwen2.5-14B-Instruct	QWE-14B
SakanaAI/TinySwallow-1.5B-Instruct	INS-1.5B
Yi-6B-Chat	YIX-6B
deepseek-ai/DeepSeek-R1-Distill-Llama-8B	BXX-8B
gemma-2-2b-it	GEM-2B
gemma-2-9b-it	GEM-9B
google/gemma-3-12b-it	ITX-12B
google/gemma-3-1b-it	ITX-1B
google/gemma-3-4b-it	ITX-4B
google/gemma-3-7b-it	ITX-7B
granite-3.0-8b-instruct	GRA-8B
meta-llama/Llama-2-13b-chat-hf	HFX-13B
meta-llama/Llama-2-7b-chat-hf	HFX-7B
meta-llama/Meta-Llama-3-70B-Instruct	INS-70B
meta-llama/Meta-Llama-3-8B-Instruct	INS-8B
microsoft/Phi-3-mini-128k-instruct	INS-128K
microsoft/Phi-3-mini-4k-instruct	INS-4K
mistralai/Mistral-7B-Instruct-v0.3	VXX-7B
nvdiia/Nemotron-Mini-4B-Instruct	INS-4B

TABLE 3: Model ID Mapping with Alphabetical Labels

Model ID	Letter
Llama3-8B	A
gemma3-4b	B
gemma2-9b	C
qwen3-8b	D
qwen2.5-7b	E
deepseek-llama8b	F
mistral-7bv3	G
synlogic-7b	H
deepseek-qwen1.5b	I
Llama2-7B	J

Unsafe Rate. This metric is computed using the safety classifications provided by `Qwen3Guard`. A model output is counted as unsafe whenever the guard model labels it as “Unsafe.” Formally,

$$\text{Unsafe Rate} = \frac{N_{\text{Unsafe}}}{N_{\text{Total}}},$$

where N_{Unsafe} denotes the number of responses flagged as Unsafe by the guard model, and N_{Total} denotes the total number of model responses evaluated.

Refusal Rate. This metric is based on refusal-style keyword matching. A model response is counted as a refusal if it contains typical refusal patterns such as “I’m sorry”, “I

cannot comply”, “I refuse to answer”, or similar formulations. Formally,

$$\text{Refusal Rate} = \frac{N_{\text{Refusal}}}{N_{\text{Total}}},$$

where N_{Refusal} denotes the number of responses that match the refusal keyword patterns.

Complementarity. These two metrics capture opposite behavioral tendencies and are therefore complementary. Lower *Unsafe Rate* indicates stronger safety, while lower *Refusal Rate* indicates better helpfulness and less over-defensiveness. A high Unsafe Rate signals safety failures, whereas a high Refusal Rate reflects an overly conservative model that rejects too many user requests.